THE JOURNAL OF PHYSICAL CHEMISTRY A

Article

pubs.acs.org/JPCA

Tuning the Emission Properties of Fluorescent Ligands by Changing pH: The Unusual Case of an Acridine-Containing Polyamine Macrocycle

Stefano Puccioni,[†] Carla Bazzicalupi,[†] Andrea Bencini,[†] Claudia Giorgi,*[,†] Barbara Valtancoli,[†] Greta De Filippo,[‡] Vito Lippolis,[‡] Pier Remigio Salvi,[†,§] Giangaetano Pietraperzia,[†,§] Riccardo Chelli,*[,†,§] and Cristina Gellini*[,†,§]

[†]Dipartimento di Chimica "Ugo Schiff", Università di Firenze, Via della Lastruccia 3, 50019 Sesto Fiorentino, Firenze, Italy

[‡]Dipartimento di Scienze Chimiche e Geologiche, Università di Cagliari, S.S. 554 bivio per Sestu, 09042 Monserrato, Cagliari, Italy

[§]European Laboratory for Nonlinear Spectroscopy (LENS), Via Nello Carrara 1, 50019 Sesto Fiorentino, Firenze, Italy

Supporting Information

ABSTRACT: Synthesis and characterization of a new macrocyclic compound, composed by a triethylentetraamine chain linking the 4 and 5 positions of an acridine moiety, are reported. The molecule, devised as a fluorescent chemosensor for anions, has revealed an intriguing pH-dependent spectroscopic behavior, whose features are the specific object of this article. Ligand protonation in aqueous solution has been analyzed by means of potentiometric, ^{1}H NMR, UV−vis, and fluorescence emission measurements. The molecule binds up to four protons in the pH range 2−11. Protonation takes place on the aliphatic tetraamine chain, while the acridine nitrogen does not participate to proton binding even at very low pH. Differently from acridine, the UV−vis spectra are almost unaffected by the pH. On the opposite, the emission spectra are strongly pH-dependent. In fact, at low pH values, the spectra show a blue-shifted emission, resembling that of unprotonated acridine, while at slightly acidic and alkaline pH the fluorescence features a red-shifted band similar to that of acridinium cation. This unusual behavior occurs in the mono-, bi-, and triprotonated forms of the compound and is interpreted as due to an excited state proton transfer from an aliphatic ammonium group adjacent to the acridine moiety to the acridine nitrogen. In the fully protonated state, this process is prevented owing to unfavorable molecular arrangements mainly determined by electrostatic repulsions. This interpretation is supported by quantum mechanical calculations as well as molecular dynamics simulations.

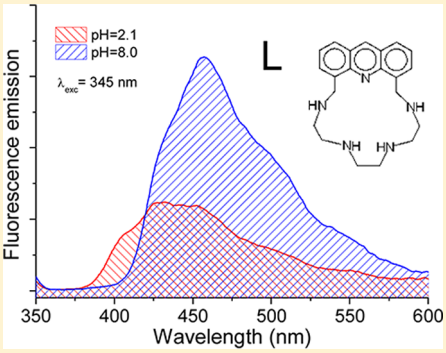

1. INTRODUCTION

In the last years, increasing interest has been devoted to acridine and its derivatives, due to their peculiar chemical[1−3] and photophysical properties[2−15] as well as to the biological activity[16,17] imparted by the planar tricyclic structure. From this point of view, the known capability of acridine to intercalate between DNA base pairs has been largely exploited to develop new agents with anticancer activity.[16−25] The first and most cited example is amsacrine,[20,22] which contains a 4-amino-3-methoxyphenyl-methanesulfonamide function linked to the 9 position of acridine. This molecule, used in clinics since 1976, is the first totally synthetic drug of DNA intercalating type, the beneficial effect in cancer therapy being due to its interaction with Topo-II-DNA complex.[20,22,26,27] Its success has led to the synthesis of a number of similar compounds for pharmacological purposes and presently acridine derivatives are used not only as antitumor drugs, but also as antibacterial and antimicrobial agents.[16−18] Acridine-based compounds normally display an intense fluorescence, which is strongly sensitive to the polarity of the medium. Interaction within DNA/RNA strands is therefore often accompanied by changes of the emission wavelengths and/or fluorescence intensity.[22,23] As a consequence, acridine-based compounds, in particular 3,6-diamino derivatives, such as acridine-orange and proflavine, are used as fluorescent probes for DNA and RNA in a number of biological procedures.[28,29] Luminescence is also strongly affected by protonation of the acridine nitrogen.[6−9,15] For instance, protonation of the acridine nitrogen in aqueous solution occurs at acidic pH and gives rise to a 40 nm red-shift of the original emission band of acridine at 430 nm.

The luminescence properties of acridine and its derivatives and their sensitivity to substrate coordination make them promising candidates to develop new fluorescent chemosensors for analytes in aqueous solution.[30−32] Chemosensors are normally constituted by a binding moiety capable to recognize a targeted substrate, linked via a spacer to a signaling units for

Received: February 13, 2013
Revised: April 11, 2013
Published: April 15, 2013

example, a fluorogenic molecule whose fluorescence emission is quantitatively altered by the binding event.[33] From this point of view, polyamine macrocycles have been revealed to be versatile binding units for metal cations[33−42] and, more recently, also for anionic species.[43,44] In fact, they can easily protonate affording polyammonium cation at neutral pH values, capable to bind anions via charge−charge or hydrogen bonding (H-bonding) interactions. Furthermore, compared to open-chain polyamines, their cyclic structure leads to an increased density of positive charge on the receptor, strengthening the overall host−guest interaction. In this context, the insertion of a signaling unit, most often a fluorescent heteroaromatic fragment, as an integral part of the polyamine macrocyclic structure, represents one of the approaches to the development of anion chemosensors.[43−57]

With this in mind, we have synthesized the new receptor 1-(6,7)-acridina-3,6,9,12-tetraazatridecaphane (from now on denoted as L), composed by a triethylentetraamine chain linked to the 4,5 positions of an acridine moiety through two methylene spacers (Figure 1). It is now accepted that the binding affinity for anions of a polyamine receptor does not only depend on the facile protonation of the amino groups in solution, but also on the structural organization of the ammonium groups within the macrocyclic structure. In fact, selective anion binding requires an optimal stereochemical fitting between the binding sites of the two partners in the host−guest interaction. At the same time, protonation of the receptor can strongly affect its luminescence properties. Therefore, the investigation of the structural and photophysical properties of the polyammonium cations generated by protonation is a necessary preliminary analysis in the study of the anion chemosensing capability of new receptors. In the present case, we noted that at strongly acidic pH the L receptor displays an emission band peaked at 430 nm, while in slightly alkaline medium the fluorescence emission is red-shifted at 460 nm, which is the opposite behavior observed for acridine.[7,10] Stimulated by these unexpected observations, we decided to focus our efforts on a multidisciplinary study of the structural and photophysical properties of the receptor L at different pH values, by coupling potentiometric, ^{1}H NMR, UV−vis absorption and fluorescence emission measurements in aqueous solution with quantum mechanical (QM) calculations and molecular dynamics (MD) simulations.

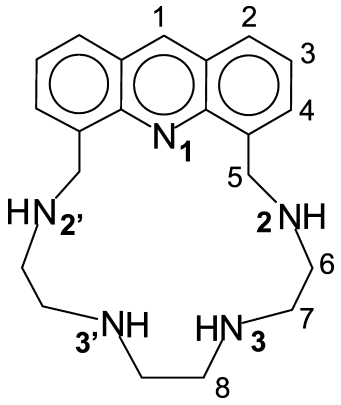

Figure 1. 1-(6,7)-Acridina-3,6,9,12-tetraazatridecaphane (L) structure with atom labeling for the purpose of the present paper.

2. EXPERIMENTAL SECTION

2.1. Synthesis of the Ligand. 4,5-Dibromomethylacridine **1** has been synthesized using a modification of the procedure developed by Di Giorgio et al.[58] 1,4,7,10-Tetratosyl-1,4,7,10-tetraazadecane **2** was obtained as previously reported.[59] The synthetic pathway to obtain L is depicted in Figure 2.

*3,6,9,12-Tosyl-1-(6,7)-acridina-3,6,9,12-tetraazatridecaphane (Compound **3** in Figure 2).* The tosylated amine **2** (500 mg, 0.655 mmol) and K_2CO_3 (1.5 g, 11.0 mmol) were suspended in refluxing CH_3CN (20 mL). A solution of **1** (240 mg, 0.655 mmol) in CH_3CN (40 mL) was then added dropwise in 2 h to the resulting mixture. After completing the addition, the suspension was refluxed for 22 h and then filtered. The solution was evaporated in vacuum to yield the crude product which was chromatographated on activated alumina (II/III) CH_2Cl_2-ethyl acetate 10:1 mixture. The eluted fractions were collected and evaporated to dryness to afford **3** as a colorless solid (310 mg, 49%). Anal. Calcd for $C_{49}H_{51}N_5S_4O_8$ C, 60.91; H, 5.32; N, 7.25. Found C, 60.83; H, 5.33; N, 7.22. ^{1}H NMR ($CDCl_3$) δ 2.38 (s, 6H), 2.42 (s, 6H), 2.54 (t, 4H), 2.70 (t, 4H), 3.39 (t, 4H), 5.18 (s, 4H), 7.21 (d, 4H), 7.32 (d, 4H), 7.42 (d, 4H), 7.54 (dd, 2H), 7.76 (d, 4H), 7.89 (d, 2H),

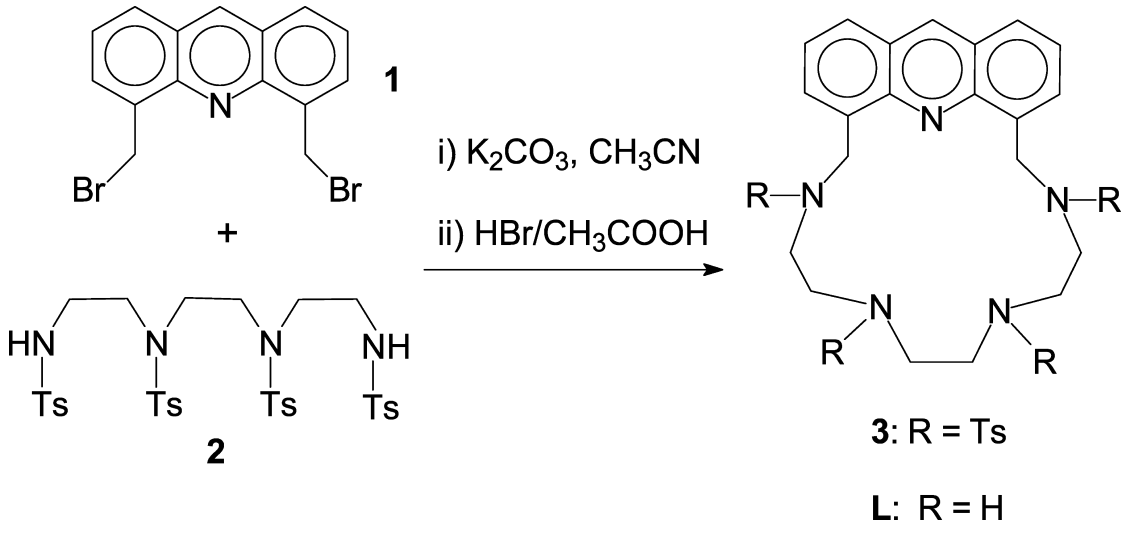

Figure 2. Synthesis scheme of L.

dx.doi.org/10.1021/jp4015756 | J. Phys. Chem. A 2013, 117, 3798−3808

7.95 (d, 2H), 8.72 (s, 1H). ^{13}C NMR ($CDCl_3$) δ 146.99, 143.53, 143.44, 137.17, 135.66, 135.19, 134.84, 132.69, 129.98, 129.95, 129.77, 129.74, 128.78, 127.71, 127.69, 127.47, 126.60, 126.06, 49.55, 49.44, 49.18, 48.22, 21.67, 21.64.

1-(6,7)-Acridina-3,6,9,12-tetraazatridecaphane Tetrahydrobromide Pentahydrate (L·4HBr·5H$_2$O). Tetratosylated macrocycle **3** (310 mg, 0.321 mmol) and phenol (3.5 g, 37 mmol) were dissolved in HBr/CH_3COOH (33%, 15 mL). The solution was stirred at 90 °C for 22 h. The resulting suspension was filtered, and the solid was washed with CH_2Cl_2 for several times. The yellowish solid was recrystallized from an ethanol/water mixture (20 mL) in the presence of few drops of 48% HBr to give L as the tetrahydrobromide salt L·4HBr·5H_2O (92 mg, 38%). Anal. Calcd for $C_{21}H_{41}N_4O_5Br_4$ C, 33.05; H, 5.42; N, 9.18. C, 33.12; H, 5.43; N, 9.34. ^{1}H NMR (D_2O, pH 1.9) δ 9.21 (s, 1H), 8.30 (d, 2H), 8.05 (d, 2H), 7.71 (dd, 2H), 5.07 (s, 4H), 3.57 (t, 4H), 3.35 (t, 4H), 3.13 (s, 4H). ^{13}C NMR (D_2O, pH 1.9) δ 145.84, 139.06, 133.91, 131.51, 128.08, 126.82, 126.17, 59.92, 47.94, 44.61, 43.92, 43.48. MS (Supporting Information, SI) m/z 350 $(M + H)^+$.

L·4HBr·2H$_2$O Crystal. Crystals suitable for X-ray analysis of the dihydrate salt L·4HBr·2H_2O were prepared in 89% yield by slow evaporation at room temperature of an aqueous solution of L (0.01 M), acidified with 1 M HBr up to pH 2, in the presence of a fifty-fold excess of NaBr. Anal. Calcd for $C_{21}H_{35}N_5O_2Br_4$ C, 33.75; H, 5.00; N, 9.93. Found C, 33.82; H, 5.14; N, 9.73.

2.2. X-ray Structure Determination of L·4HBr·2H$_2$O. Crystal data for L·4HBr·2H_2O: $(C_{21}H_{35}Br_4N_5O_2)_2$, MW = 1418.36, orthorhombic, *Pbca*, a = 22.535(1) Å, b = 13.0247(9) Å, c = 39.473(3) Å, V = 11586(1) Å^3, Z = 8, T = 150 K, μ(Cu K_α) = 6.986 mm^{-1}, 60477 reflections measured, 6837 unique (R(int) = 0.0884). The final agreement factors were R_1 = 0.0785 (5146 data with $I > 2\sigma(I)$) and $wR(F^2)$ was 0.2460 (all data). Due to the somewhat low quality of the crystal, reflections were used only up to 0.9 Å resolution ($2\theta_{max}$ = 118°) in structure solution and refinement. The structures were solved by direct methods (SIR2004)[60] and refined using SHELX-97.[61] All of the non-hydrogen atoms were anisotropically refined, while the hydrogen atoms were introduced in calculated positions and their coordinates and thermal parameters refined according to the linked atom. The oxygen atoms belonging to the solvent molecules were refined using partial population parameters. Residual electron density near a disordered water oxygen remains at the end of refinement. Attempts to introduce the residual density as an additional crystallization water molecule were unfruitful. The CIF file for this structure has been deposited to the Cambridge Crystallographic Data Center, CCDC deposition no. 911103.

2.3. Potentiometric Measurements. Potentiometric measurements were carried out in degassed 0.1 M N-$(CH_3)_4NO_3$ aqueous solutions, at 25 °C by using equipment and procedure described in ref 62. The combined Ingold 405 S7/120 electrode was calibrated as a hydrogen concentration probe by titrating known amounts of HNO_3 with CO_2-free $N(CH_3)_4OH$ solutions and determining the equivalent point by the Gran's method,[63] which allows us to determine the standard potential $E°$, and the ionic product of water (pK_w = 13.83(1) at 25 °C in 0.1 M solution of $N(CH_3)_4NO_3$). The concentration of L was generally 10^{-3} M. At least three measurements (about 100 data points each one) were performed in the pH range 2−11, and the relevant electromotive force data were treated by means of the computer program HYPERQUAD.[64]

2.4. NMR Measurements. ^{1}H (400 MHz) and ^{13}C (100 MHz) in $CDCl_3$ and D_2O solutions at different pH values were recorded at 25 °C on a 400 MHz Bruker Avance II spectrometer. To adjust the pD, small amounts of 0.01 M NaOD and DCl were added to the solution containing L. The pH was calculated by the measured pD values by using the relationship[65] pH = pD − 0.40.

2.5. Absorption and Emission Spectra. The absorption spectra of L (3×10^{-5} M) and acridine (8×10^{-6} M) in water solution at various pH have been measured with a Cary 5 spectrophotometer in the spectral range 200−700 nm. The spectral bandwidth was set to 2 nm and the optical path length was 1 cm. Fluorescence emission has been measured on the same solutions by means of a Perkin-Elmer LS55 spectrophotofluorimeter, exciting at 345 nm and collecting the emission in the range 350−680 nm. Attenuating the sample emissions by using a T = 1% neutral density filter allows to measure all of the samples in the same experimental conditions, i.e., excitation and emission slits fixed at 10 nm. Emission spectra have been corrected for the response of the photomultiplier. The absence of exciplexes or aggregation effects have been checked by diluting the solutions down to 8×10^{-7} M without observing any change both in the absorption and emission features. In recording the spectra at different pH, the examined pH values for L are 1.1, 2.1, 5.0, 8.2, and 12.0, while for acridine they are 2.5, 5.0, and 8.0. The pH values have been chosen to roughly maximize the presence of only one species in solution, as established from potentiometric experiments. Each pH value has been adjusted adding concentrated NaOH or CH_3SO_3H solutions.

2.6. Computational Methods. QM calculations have been performed on neutral L and protonated forms of L, H_nL^{n+} with n = 1, 2, 3, 4, the protonation sites being established according to potentiometric and NMR measurements. In the HL^+ and H_2L^{2+} species the acidic protons are localized, respectively, on one and both the amino groups adjacent to the acridine moiety (N2 and N2′; see Figure 1 for labeling), while in H_3L^{3+} and H_4L^{4+} the additional acidic protons are positioned on the remaining N3 and N3′ aliphatic amine functions. The L and H_nL^{n+} configurations subject to structural QM optimization have been obtained from a quality threshold clustering[66] analysis applied to a collection of conformations taken from serial-generalized ensemble MD simulations[67−69] of L and H_nL^{n+} water solutions at room conditions. For each compound, the configuration representative of the most populated cluster has been taken. Details of clustering analysis and MD simulations are reported in the Supporting Information. MD simulations have been performed using the ORAC program.[70] The ground state structures of L and H_nL^{n+} have been achieved through energy minimization using density functional theory with the B3LYP functional and 6-31++G(d,p) basis set. The minimum-energy structures of the species with acridine in its protonated form have also been determined at the same level of theory. Their initial structures correspond to the ground-state L and H_nL^{n+} species, by moving a proton from the N2 or N2′ amino group to the N1 nitrogen. Electronic energies for the $S_0 \rightarrow S_1$ vertical transition are calculated on chain-protonated and acridine-protonated structures of H_nL^{n+} using time-dependent density functional theory[71,72] with the same functional and basis set. The excitation energies have been calculated promoting electrons from the 27 highest-energy valence

dx.doi.org/10.1021/jp4015756 | J. Phys. Chem. A 2013, 117, 3798−3808

orbitals to all 555 virtual orbitals. All calculations have been performed using the Gaussian09 program,[73] whether in vacuum or using the polarizable continuum model with dielectric constant of water.[74]

3. RESULTS AND DISCUSSION

3.1. Synthesis. Macrocycle L was obtained by using a modification of the Richman and Atkins procedure[75] (Figure 2). Reaction of the acridine dibromomethyl derivated **1** with the tosylated tetraamine **2** in CH_3CN in the presence of K_2CO_3 as base, affords, after purification by chromatography, the tosylated macrocycle **3**. Finally, removal of the tosyl groups was performed in HBr/CH_3COOH in the presence of phenol as antioxidant, as the commonly used deprotection in concentrated H_2SO_4 leads to the decomposition of the acridine moiety.[75] The macrocycle L was then precipitated as tetrahydrobromide salt by addition of CH_2Cl_2 to its solution in HBr/CH_3COOH. Crystals of the $L{\cdot}4HBr{\cdot}2H_2O$ salt, suitable for crystallographic analysis, were obtained by slow evaporation of an aqueous solution of L at pH 2 in the presence of a large excess of NaBr.

3.2. Crystal Structure of $L{\cdot}4HBr{\cdot}2H_2O$. The crystal structure consists of H_4L^{4+} cations, bromide ions, and water molecules. The asymmetric unit contains two H_4L^{4+} cations (a and b units in Figure 3), coupled by π-stacking interactions between the two acridine moieties. In Figure 3, an ORTEP drawing of the crystal structure is reported including symmetry related bromide ions (Br3′, Br2′, Br5′, Br6′, and Br8″). Each H_4L^{4+} unit is almost planar as revealed by the angle between the mean planes of acridine and macrocycle chain. The latter is defined by the C and N atoms of the aliphatic chain plus those of acridine closing the cycle. The angle results 4.0° for the a unit and 5.2° for the b unit, indicating a nearly flat conformation. The two acridine units are partially overlapped and parallel, accounting for a face-to-face π-stacking interaction. The angle between the acridine planes is 1.6° and the interplanar distance 3.3 Å, while the centroids of the central rings of the two acridine units are 1.6 Å shifted to each other. The two aliphatic chains point in opposite directions and are involved in a dense H-bonding network with bromide ions and water molecules. Although the Fourier difference map does not allow to determine the position of hydrogen atoms, it is to be noted that all the aliphatic nitrogens are involved in two or more strong H-bond interactions with bromide ions and, in the case of N3a, N3′a, N2′b, and N3b, with water molecules. Acridine is not involved in H-bonding either with bromide ions or water molecules. This suggests that all aliphatic nitrogen atoms are likely to be in their protonated form, while the acridine nitrogen remains not protonated. Only a weak H-bond between the acridine nitrogen and a single benzylic ammonium group of each macrocyclic unit is formed. In fact, both N2a···N1a and N2b···N1b distances are 3.07 Å, while the N2a-H···N1a and N2b-H···N1b angles are 122.9(6)° and 121.8(5)°, respectively, far from the optimal value of 180°. Furthermore, both the aliphatic N2a and N2b amino groups give rise to two additional interactions with two bromine ions (N2a···Br3 = 3.30(1) Å, N2a···Br4 = 3.61(1) Å, N2b···Br2 = 3.233(8) Å, N2b···Br1 = 3.328(8) Å), accounting for their protonation and ruling out protonation of acridine.

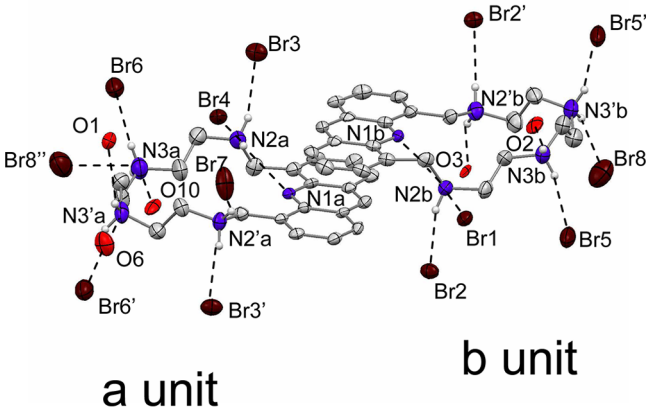

Figure 3. ORTEP drawing of the $L{\cdot}4HBr{\cdot}2H_2O$ X-ray structure, displaying the dense H-bonding network formed by the two cations, bromide ions and water molecules. Symmetry operators: $'-x + 1/2, +y + 1/2, +z$; $''x, -y + 1/2, +z - 1/2$. Relevant distances (Å) are: N2a···Br3 = 3.30(1), N2a···Br4 = 3.61(1), N2a···N1a = 3.07(1), N3a···O10 = 2.87(3), N3a···Br6 = 3.26(1), N3a···Br8″ = 3.39(1), N3′a···O6 = 2.91(2), N3′a···O1 = 3.40(1), N3′a···Br6′ = 3.37(1), N2′a···Br7 = 3.26(8), N2′a···Br3′ = 3.24(8), N2′b···O3 = 2.79(2), N2′b···Br2′ = 3.34(9), N3′b···Br8 = 3.29(1), N3′b···Br5′ = 3.24(1), N3b···Br5 = 3.24(1), N3b···O2 = 3.00(2), N2b···Br2 = 3.233(8), N2b···Br1 = 3.328(8), N2b···N1b = 3.07(1).

3.3. Potentiometric and ^{1}H NMR Study of the Ligand Protonation. Although acridine suffers poor solubility in water, the presence of a hydrophilic tetraamine chain in L ensures high solubility and allows for the determination of its protonation constants via potentiometric titrations. The stepwise protonation constants of L (log *K*), potentiometrically determined at 25 °C in 0.1 M solution of $N(CH_3)_4NO_3$, are reported in Table 1. As normally found in polyamine-based compounds, facile protonation of the amino groups can occur in aqueous solutions. Accordingly, L can bind up to four acidic protons in the investigated pH range 2−11, affording different protonated species from alkaline to acidic pH values (Figure 4). L possesses four amino groups and the acridine nitrogen as potential binding sites for protons. On the other hand, the first two protonation constants are in the range normally observed for aliphatic amines[76] and far higher than that observed for acridine[7,76,77] (log *K* = 5.4), suggesting that the corresponding protonation steps occur on the polyamine chain. Conversely, the values of the remaining protonation constants are similar or lower than that of acridine (Table 1) and, in principle, the corresponding protonation steps may involve either the amino groups of the aliphatic chain or the acridine nitrogen.

Table 1. Protonation Constants (log *K*) Related to the Various Equilibria Involving Neutral and Protonated Forms of L[a]

equilibrium	log *K*
$L + H^+ = HL^+$	10.24 (6)
$HL^+ + H^+ = H_2L^{2+}$	9.44 (5)
$H_2L^{2+} + H^+ = H_3L^{3+}$	5.91 (9)
$H_3L^{3+} + H^+ = H_4L^{4+}$	3.36 (9)

[a]The L concentration is 10^{-3} M in 0.1 M aqueous solution of $N(CH_3)_4NO_3$ at 25 °C. Values in parentheses are errors on the last significant digit.

dx.doi.org/10.1021/jp4015756 | J. Phys. Chem. A 2013, 117, 3798−3808

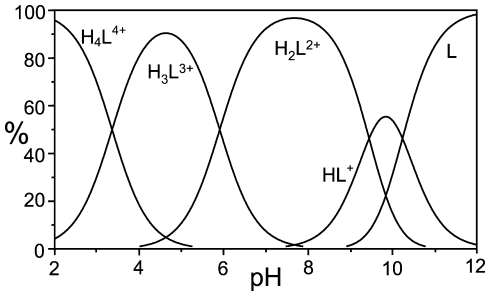

Figure 4. Distribution diagram of the protonation states of L (10^{-3} M) in 0.1 M solution of $N(CH_3)_4NO_3$ at 25 °C.

A qualitative description of the successive protonation steps of L can be gained by ^{1}H NMR spectra recorded at different pH values. It is known, in fact, that proton binding is accompanied by marked downfield shifts of the ^{1}H resonances of the methylene groups in α-position with respect to the aliphatic nitrogen involved in the protonation process. These spectral changes can be used as diagnostic tool to monitor the protonation process. The ^{1}H NMR spectrum of L at pH 12, where the free amine predominates, features a set of eight signals, four for the acridine moiety [a singlet at 7.95 ppm (assigned to the H1 hydrogen, see Figure 1 for labeling), two doublets at 7.73 and 7.48 ppm (the hydrogen atoms H2 and H3) and a doublet of doublets at 7.28 (H4)], and four for the aliphatic chain [two singlets at 3.80 and 2.45 ppm (H5 and H8) and two multiplets at 2.60 and 2.45 ppm (H6 and H7)]. These spectral features account for a time-averaged C_{2v} symmetry of the molecule, which is preserved throughout all the investigated pH range. As shown in Figure 5, formation of the mono- and

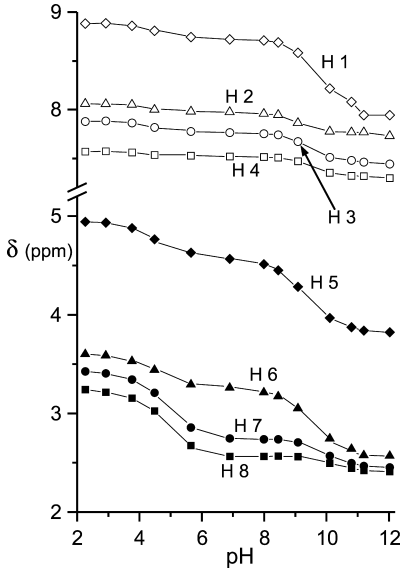

Figure 5. ^{1}H-NMR signals of L as a function of pH (see Figure 1 for labeling).

diprotonated species, HL^+ and H_2L^{2+}, in the 7−11 pH range is accompanied by marked downfield shift of the signals of the methylene protons H5 and H6, adjacent to the amino groups N2 and N2′. A minor shift is observed for the resonances of H7 and H8, close to central amino groups of the aliphatic chain, N3 and N3′. Finally, the formation of the HL^+ and H_2L^{2+} species also induces downfield shifts for the resonances of the aromatic protons, in particular for the H1 signal. It is known that in macrocyclic polyamines, including those containing aromatic or heteroaromatic rings, the acidic protons are often delocalized over the whole set of nitrogens or shared via hydrogen bonding between different amino groups.[78] This probably also occurs in the present case. However, the structural characteristics of the macrocycle and the nature of the aromatic ring may influence the distribution of the acidic protons within the cyclic framework. For instance, in polyamine macrocycle containing phenanthroline[79] or dipyridine[80] units, the first protonation steps often occur on the amino groups far from the heteroaromatic moieties, whereas preferential protonation of the benzylic amines has been observed in benzene-[81,82] or thiophene-containing[83] polyazamacrocycles. In the present case, the larger shift observed for the signals of the methylene groups H5 and H6 leads us to propose that in the H_2L^{2+} species the two acidic protons are located, to a greater extent, on the N2 and N2′ nitrogens. This would also ensure a reduction of the electrostatic repulsions between the two ammonium groups, which result far apart from each other, separated by the large acridine unit. However, a minor localization of positive charge on the N3 and N3′ amino groups and/or on the acridine nitrogen cannot be ruled out. Binding of the third and fourth acidic protons below pH 6 gives rise to the formation of the H_3L^{3+} and H_4L^{4+} forms. This process is accompanied by a relevant downfield shift of the signals of the methylene groups H7 and H8, adjacent to the N3 and N3′ nitrogens, while only minor shifts are observed for the remaining signals, including those of acridine. Therefore, the last two protonation steps are likely to mainly involve the two central amino groups of the aliphatic chain.

These data indicate that, throughout all of the considered pH range, acridine is never directly involved in proton binding, even at strongly acidic pH, probably due to the presence of a high density of positive charge on the side chain that prevents acridine protonation. This finding is supported by the crystal structure of the H_4L^{4+} cation, which shows that acridine is unprotonated in this form, at least in the solid state.

3.4. Absorption and Fluorescence Spectroscopy. The acid−base equilibria of L have been characterized by absorption and fluorescence spectra. It is convenient for their interpretation the comparison with equivalent data on acridine in aqueous solution, whose dependence on pH is well-known.[6,7] Our own results on acridine, obtained for the purpose of the present paper and shown in Figures 6a and 7a, agree satisfactorily with past reports.[8,9] The lowest energy absorption spectrum of acridine has been discussed in terms of two transitions, the first of $n\pi^*$ and the second of $\pi\pi^*$ character, whose relative energies are sensitive to the environment polarity. In polar solvents the lowest transition has been conclusively reported to be of $\pi\pi^*$ nature.[10] The absorption onset shifts from ∼380 nm at alkaline and neutral pH, where the unprotonated form predominates, to ∼430 nm at pH 2.5 where the acridinium ion is in the largest concentration. The mirror symmetry between fluorescence and absorption spectra and the comparable red shift observed in the fluorescence spectra are good indications for the assignment to acridine and acridinium ion of the two emissions[7,11,13] (see Figure 7a). The occurrence of the isosbestic point at 440 nm in the fluorescence spectra points to the acid−base equilibrium of acridine in solution.[12,13]

The absorption spectra of L, measured in the 250−500 nm wavelength interval at different pH values, are shown in Figure

dx.doi.org/10.1021/jp4015756 | J. Phys. Chem. A 2013, 117, 3798−3808

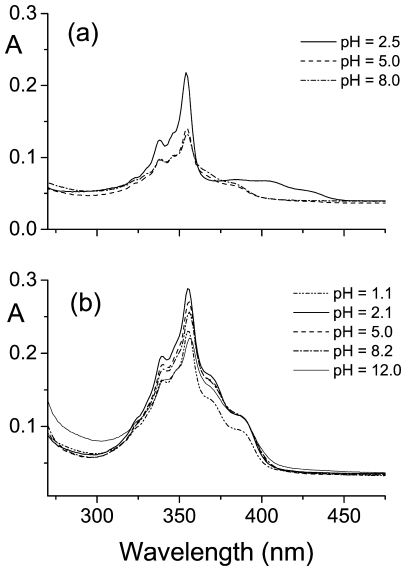

Figure 6. UV−vis absorption spectra of aqueous solution of acridine (panel a, $C = 3 \times 10^{-5}$ M) and L (panel b, $C = 8 \times 10^{-6}$ M) in aqueous solution at different pH values.

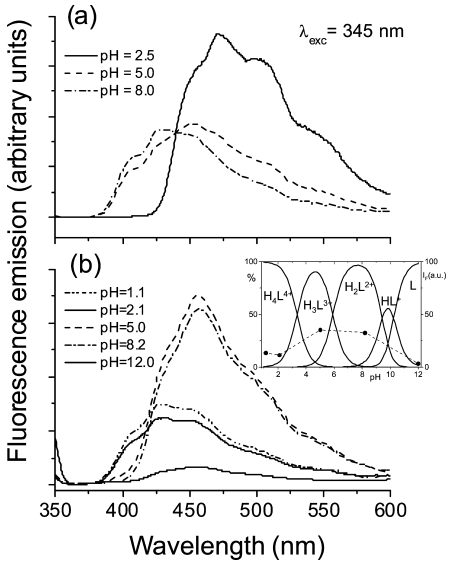

Figure 7. Fluorescence emission spectra of aqueous solution of acridine (panel a, $C = 3 \times 10^{-5}$ M) and L (panel b, $C = 8 \times 10^{-6}$ M) in aqueous solution at different pH values. The excitation wavelength is 345 nm. In the inset, the fluorescence emission intensity measured at 456 nm as a function of pH has been overlapped to the distribution diagram of the protonation states of L.

6b. The absorption is due to the aromatic chromophore. However, at variance with results on pure acridine, all of the L spectra show nearly the same absorption profile in the range 300−450 nm, irrespective of pH. Two band systems are recognized, the first with onset around 390 nm and the second with a peak at 355 nm and the associated vibronic structure, assigned as the second $\pi\pi^*$ transition of the chromophore.[8,11,84]

The fluorescence spectra are collected in Figure 7b. Exciting at 345 nm, pH dependent emissions are observed. In strongly acidic solutions (pH = 1.1 and 2.1), where the most abundant species is the tetraprotonated ligand H_4L^{4+}, the fluorescence spectrum closely resembles that of acridine in alkaline solution, with origin at 404 nm, a broad maximum at ∼430 nm and extension up to 540 nm. In slightly acidic and alkaline solutions, pH 5.0 and 8.2, where the tri- and biprotonated species, respectively, are in the largest concentration, as evidenced in the inset of Figure 7b, the fluorescence emission is enhanced and shifted to the red. Finally, in a strongly alkaline solution the same spectrum is observed, though largely depressed. Summarizing, varying the pH conditions (1) the L absorption is unaffected, while (2) the L fluorescence is reversed with respect to acridine in the sense that the spectrum at mildly acidic and alkaline pH is similar to that of acridine at acidic pH and vice versa. A second result is the absence of isosbestic points in the L fluorescence spectra, in further contrast with the acridine behavior. In agreement with potentiometric results, this indicates that the acridine chromophore is not involved in the acid−base equilibria in the ground state, and as a consequence, the acridinium form of the chromophore is not formed at any pH. Being the aromatic chromophore responsible of the absorption spectrum and the acridine form of the ligand occurring all over the investigated pH range, the independence of the absorption spectrum on pH easily follows.

As to point (2), we start with the consideration that acid−base properties of acridine in the lowest $\pi\pi^*$ state differ from those of the ground state. Acridine is significantly more basic upon excitation, pK_a = 9.2, than in the ground state, pK_a = 5.4.[6,7,9] Second, the pK_a value of the excited state is comparable to that of aliphatic amino groups in the ground state.[76] This suggests that a similar pK_a increase may occur also in the acridine unit of L favoring the intramolecular excited state proton transfer from the ammonium group of the aliphatic chain to the nitrogen of the acridine unit, as it has been reported for other acridine derivatives.[6,7,14,15] With the indication from now on of the "neutral-like" and "protonated-like" structures of the ligand at the acridine nitrogen as **A** and **B**, respectively, the process, likely to involve the protonated amino groups N2 and N2′ (see Figure 1 for atom labeling), can be described schematically as excitation of the ligand in the "neutral-like" form, **A** → **A***, followed by proton transfer to the "protonated-like" form in the excited state, **A*** → **B***, and fluorescence emission, **B*** → **B** (see Figure 8). **A** is recovered

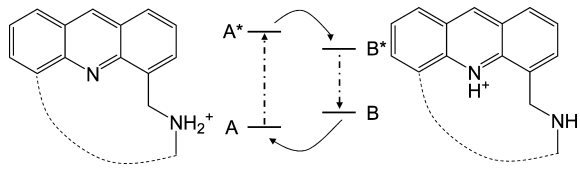

Figure 8. Schematic representation of the excited state proton transfer from the **A*** to **B***. The relevant parts of the **A** and **B** geometries are also sketched, highlighting the role of the N2 amino group in the proton transfer process.

in the final **B** → **A** process if the reasonable assumption is made that the ground state pK_a values of L are not substantially changed with respect to those of acridine and the aliphatic amino groups. Looking at Figure 7b, it is seen that our model is consistent with the fluorescence behavior at pH 5.0 and 8.2, that is, exciting the tri- and biprotonated species, but less convincing for the fluorescence spectra at high and low pH values. In strongly alkaline solution, **A*** → **A** fluorescence is expected because unprotonated ligand is predominant and hence no proton transfer can occur. On the contrary, this fluorescence is not observed. The inhibition is related, as often

dx.doi.org/10.1021/jp4015756 | J. Phys. Chem. A 2013, 117, 3798−3808

reported for unprotonated polyamine-based fluorescent chemosensors,[30,41] to a photoinduced electron transfer from the nonbonding lone pair of the amino nitrogen to the excited chromophore. The emission at pH 12.0 is thus ascribed to the presence of a minor amount of the HL^+ cation fluorescing according to the above-mentioned scheme, **A** → **A*** → **B*** → **B**. On the other pH side, in strongly acidic solution the tetraprotonated form largely outweighs all of the others so that in principle the proton transfer may occur in the excited state. However, in this case only the **A*** → **A** fluorescence is observed, and the absence of the **B*** → **B** emission has been tentatively related to the activation energy of the **A*** → **B*** process, sufficiently high to prevent the excited state proton transfer.

3.5. Ab Initio and MD Simulation Results. Our model implies that the **A** form lies at energy lower than **B** for all protonated species. In order to validate this hypothesis QM calculations have been performed on L and H_nL^{n+} species, according to the procedure outlined in Section 2.6. The optimized structures correspond to energy minima, given the absence of imaginary frequencies in the calculated vibrational modes. Due to the multitude of conformational isomers relative to L and H_nL^{n+}, only the structures which, according to the MD simulations, correspond to the most populated isomers at room temperature will be presently considered as starting structures for energy optimizations. The optimized configurations of L, H_2L^{2+}, and H_4L^{4+} calculated in the polarizable continuum model approximation are reported in Figure 9 as representative results. Starting with the calculations in vacuum shown in Table 2, the highly unsymmetrical **A** and **B** structures of HL^+ and H_2L^{2+} are almost at the same energy, while the **B** forms of H_3L^{3+} and H_4L^{4+} are markedly more stable than **A**. The result is

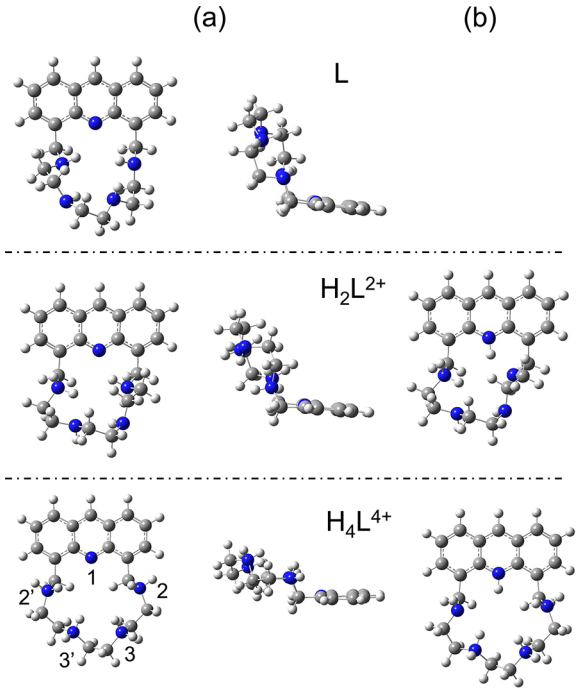

Figure 9. Calculated structures of L and the **A**-type H_2L^{2+} and H_4L^{4+} cations (a: left, top view; middle, side view) and of the **B**-type H_2L^{2+} and H_4L^{4+} cations (b: right, top view). Significant distances (Å) between non adjacent nitrogen atoms follow. **A**-type H_2L^{2+} cation: N2···N2′ = 4.41, N3···N2′ = 4.62, N2···N3′ = 4.56; **A**-type H_4L^{4+} cation: N2···N2′ = 6.14, N3···N2′ = 5.77, N2···N3′ = 5.34.

Table 2. Calculated Energy Differences $\Delta E_{BA} = E_B - E_A$ (eV) between A- and B-Type Ground State Structures in Vacuum and in Water Polarizable Continuum Medium (See Text for the Definition of the A and B Structures). Last Row: ΔE_{BA} Relative to the Water Complexes of A and B in the Polarizable Medium

ΔE_{BA}	HL^+	H_2L^{2+}	H_3L^{3+}	H_4L^{4+}
vacuum	−0.02	0.04	−0.74	−1.09
polarizable medium	0.23	0.20	0.01	−0.15
water complex	0.42	0.36	0.21	0.07

reasonably related to the nonbonded interactions N···H between nitrogen and hydrogen atoms of adjacent amino groups in the **A** and **B** forms. The energy pattern drastically changes when H_nL^{n+} is immersed in a polarizable continuum (see Table 2). A close inspection of H_nL^{n+} structures (see Figure 9) indicates that increasing the positive charge on the polyamine chain the macrocycle expands,[85−88] and as a consequence, nonbonded interactions are weakened, reducing the molecular folding between the acridine ring and the average polyamine plane. The overall effect is to stabilize the **A** form, being the solvent interaction stronger with the outer ammonium group along the chain than with the inner NH^+ acridine fragment. Referring to Table 2, all of the stabilization energies, defined as ΔE_{BA}(vacuum) − ΔE_{BA}(polarizable medium), shift in favor of **A**, as much as 0.94 eV in the case of H_4L^{4+}. Thus, from the data of Table 2 it may be seen that, at room temperature, **B** is in negligible abundance with respect to **A** for both the mono- and biprotonated species. Solvation effects are better appreciated when the solvent−solute interaction is taken into explicit account, for instance in the complex of H_nL^{n+} with one molecule of water. Now both **A** and **B** forms are in the polarizable continuum and the water molecule interacts alternatively with the N2 ammonium group (form **A**) or with the N2 amino group (form **B**). The energy differences ΔE_{BA} are found to be positive; that is, the water complexes with **A** are more stable than those with **B** for all the H_nL^{n+} species. It may be concluded that the model, in spite of its crudity, emphasizes the essential role of the interaction with the solvent in determining the invariance with pH of the absorption profiles. The QM calculated structures are available upon request.

With the acridine unit of the cromophore being responsible of the H_nL^{n+} absorption, the vertical excitation energies **A** → **A*** and **B** → **B*** from the **A** and **B** minima are only slightly perturbed by the polyamine chain. The calculated **A** → **A*** transition energies of Table 3, which are around 3.20 eV (corresponding to 388 nm excitation wavelength), match nicely the lowest energy absorption bands. The **B** → **B*** transition energies shift to the red, ∼2.92 eV (corresponding to ∼424 nm excitation wavelength), thus justifying the even larger shift of the fluorescence emission of the bi- and triprotonated species. On the contrary, the fluorescence spectrum in strongly acidic solutions overlaps quite closely that of acridine at pH 8.0, where the chromophore is unprotonated. As anticipated, we argue that the fluorescence is likely to be due to the **A*** → **A** transition ruling out the proton transfer from the aliphatic ammonium group to the acridine nitrogen in the excited state. The high energy barrier for the **A*** → **B*** proton transfer in the case of H_4L^{4+} can be roughly rationalized considering the structural arrangement of the aliphatic polyamine chain. The macrocycle cavity expands going from HL^+ to H_4L^{4+}, as

dx.doi.org/10.1021/jp4015756 | J. Phys. Chem. A 2013, 117, 3798−3808

Table 3. Vertical Transition Energies A → A* and B → B* (eV, nm in parentheses) to the Lowest ππ* Excited State of L and H_nL^{n+} in Water Polarizable Continuum Medium (See Text for the Definition of A and B Structures)

	L	HL^+	H_2L^{2+}	H_3L^{3+}	H_4L^{4+}
ΔE_{AA^*}	3.24 (382)	3.19 (389)	3.20 (388)	3.22 (385)	3.20 (388)
ΔE_{BB^*}		2.96 (419)	2.95 (421)	2.95 (421)	2.84 (436)

reported in Table 4. The distances between N1 and the aliphatic nitrogens are steadily growing from the mono- to the tetraprotonated species, and on the other hand, the N1···H2 distances are remarkably much shorter for H_2L^{2+} and H_3L^{3+}, 2.03 Å and 2.55 Å, respectively, than for H_4L^{4+}, 3.51 Å. The peculiar properties of H_4L^{4+} with respect to the other protonated species come to strong evidence also recurring to structural results obtained by MD simulations on the **A** forms of H_nL^{n+}. These are reported in Figure 10. In the upper part of the figure, the dependence of the distribution function relative to the N2−H···N1 and N2′−H···N1 nonbonded distances is plotted. Weak H···N1 bands peaked in the range 2.6−2.9 Å are formed in the case of HL^+, H_2L^{2+}, and H_3L^{3+}, whereas no such band is found for H_4L^{4+}, the first peak of the distribution being at much longer distance, ∼4 Å. A second distribution function is shown in the lower part of Figure 10, that is, that relative to the angle between the mean planes of the acridine ring and of the macrocycle chain (see Section 3.2). This function may be considered to give an estimate of the folding of the two planes in H_nL^{n+}. The single peak around 20° is the distinctive feature of the H_4L^{4+} function, which confirms that in this species the two planes are almost parallel, in excellent agreement with the indications from QM calculations.

Table 4. Distances (Å) between the Acridine Nitrogen N1 and the Amino Nitrogens N2, N3, N2′, and N3′ and between N1 and the Closest H Atoms Bound to N2 and N2′ (See Figure 1 for Atom Labeling). Structural Data from QM Calculations on L and on A-type Forms of H_nL^{n+} in Water Polarizable Continuum Medium

	N2	H2	N3	N3′	N2′	H2′
L	3.22	2.62	5.54	5.09	3.41	2.87
HL^+	3.38	2.98	5.12	5.02	3.38	4.00
H_2L^{2+}	2.87	2.03	5.25	5.47	3.71	3.53
H_3L^{3+}	3.18	2.55	5.34	5.72	3.75	3.44
H_4L^{4+}	3.80	3.51	5.38	5.82	3.98	3.81

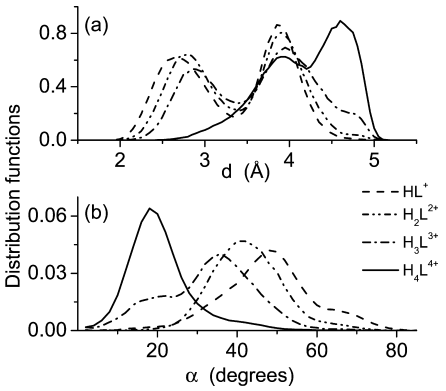

Figure 10. Upper (a): distribution functions related to N2−H···N1 and N2′−H···N1 hydrogen−nitrogen distances (Å) in H_nL^{n+} species. Lower (b): distribution functions of the angle α formed by the mean plane of the acridine ring and that of the macrocycle chain. The areas of the distribution functions have been normalized to unity.

4. CONCLUSIONS

Chemosensors are normally constituted by a signaling and a binding unit, separated by appropriate spacers. The fluorescence properties of the signaling unit and their change upon substrate binding are obvious factors which control the sensing ability of the chemosensor. The present results indicate that the fluorescence properties can be modified also by the structural arrangement of the signaling unit with respect to the binding unit. In fact, in the group of polyammonium-based fluorescent ligands, one of the most common class of anion chemosensors, macrocycle L represents an interesting case of pH controlled molecular switch. By means of potentiometric and NMR measurements the four acid−base equilibria of L have been fully characterized. Thus, anion chemosensing may be tuned along all the pH range by inducing the occurrence of one form, out of several protonated species. Further, these data together with the crystal results have been instrumental to highlight fluorescence properties of L depending on the proton transfer in the excited state from the ammonium group of the binding unit to the signaling unit. Due to this process, the fluorescence spectrum of L in slightly acidic and alkaline solutions, the most relevant pH region for anion recognition and sensing, has been correlated to that of the protonated acridine, normally not present in solution in this pH range.

Taking into account that anion binding often modifies the charge localization on the receptors, L and its protonated forms may represent a novel interesting tool to study anion chemosensing. We are currently working in this direction.

■ ASSOCIATED CONTENT

Supporting Information

Technical details of MD simulations, cluster analysis and crystal structure CIF file. This material is available free of charge via the Internet at http://pubs.acs.org.

■ AUTHOR INFORMATION

Corresponding Author

*E-mail: claudia.giorgi@unifi.it; riccardo.chelli@unifi.it; cristina.gellini@unifi.it.

Author Contributions

Designed the research: Bencini, Gellini, Lippolis, Pietraperzia. Wrote the paper: Bencini, Chelli, Gellini, Salvi. Synthesis and characterization: De Filippo, Lippolis, Puccioni. Crystallography: Bazzicalupi. Potentiometry and NMR titration: Giorgi, Valtancoli. UV−vis and fluorescence: Gellini, Pietraperzia. Calculations: Chelli, Salvi.

Notes

The authors declare no competing financial interest.

■ ACKNOWLEDGMENTS

We thank the Italian Ministero dell'Istruzione, dell'Università e della Ricerca for financial support (Project PRIN 2009, 2009Z9ASCA).

■ REFERENCES

(1) Chiron, J.; Galy, J.-P. Reactivity of the Acridine Ring: a Review. *Synthesis* **2004**, *3*, 313−325.
(2) Goncalves, M.; Sameiro, T. *Optimized UV/visible fluorescent markers*; Springer Series on Fluorescence; Springer: New York, 2010; Vol. 8, p 27.
(3) Rigler, R. Fluorescence and Single Molecule Analysis in Cell Biology. *Biochem. Biophys. Res. Commun.* **2010**, *396*, 170−175.
(4) Sarangi, M. K.; Mitra, A.; Basu, S. Prototropic Interactions of Pyrimidine Nucleic Acid Bases with Acridine: A Spectroscopic Investigation. *J. Phys. Chem. B* **2012**, *116*, 10275−10282.
(5) Hess, S.; William, W. B.; Voityuk, A. A.; Rösch, N.; Michel-Beyerle, M. E.; Ernsting, N. P.; Kovalenko, S. A.; Pérez Lustres, J. L. Excited-State Photophysics of an Acridine Derivative Selectively Intercalated in Duplex DNA. *ChemPhysChem* **2002**, *3*, 452−455.
(6) Gafni, A.; Brand, L. Excited State Proton Transfer Reactions of Acridine Studied by Nanosecond Fluorometry. *Chem. Phys. Lett.* **1978**, *58*, 346−350.
(7) Todd Ryan, E.; Xiang, T.; Johnston, K. P.; Fox, M. A. Absorption and Fluorescence Studies of Acridine in Subcritical and Supercritical Water. *J. Phys. Chem. A* **1997**, *101*, 1827−1835.
(8) Rubio-Pons, O.; Serrano-Andres, L.; Merchan, M. A Theoretical Insight into the Photophysics of Acridine. *J. Phys. Chem. A* **2001**, *105*, 9664−9673.
(9) Rak, J.; Blazejowski, J. Experimental and INDO CI Calculations of the Elecronic Absorption-Spectra of Acridine and 9-Acridinamine Free Bases and Their Protonated Forms with Regard to Tautomeric Phenomena. *J. Photochem. Photobiol. A: Chem.* **1992**, *67*, 287−299.
(10) Diverdi, L. A.; Topp, M. R. Subnanosecond Time-Resolved Fluorescence of Acridine in Solution. *J. Phys. Chem.* **1984**, *88*, 3447−3451.
(11) Negron-Encarnacion, I.; Arce, R.; Jimenez, M. Characterization of Acridine Species Adsorbed on $(NH_4)_2SO_4$, SiO_2, Al_2O_3, and MgO by Steady-State and Time-Resolved Fluorescence and Diffuse Reflectance Techniques. *J. Phys. Chem. A* **2005**, *109*, 787−797.
(12) Sarangi, M. K.; Dey, D.; Basu, S. Influence of Heterogeneity of Confined Water on Photophysical Behavior of Acridine with Amines: A Time-Resolved Fluorescence and Laser Flash Photolysis Study. *J. Phys. Chem. A* **2011**, *115*, 128−135.
(13) Sarangi, M. K.; Basu, S. Photophysical Behavior of Acridine with Amines Within the Micellar Microenvironment of SDS: A Time-Resolved Fluorescence and Laser Flash Photolysis Study. *Phys. Chem. Chem. Phys.* **2011**, *13*, 16821−16830.
(14) Gangola, P.; Joshi, N. B.; Pant, D. D. Edge excitation red-shift and excited-state proton association in acridine. *Chem. Phys. Lett.* **1979**, *60*, 329−331.
(15) Smith, C. A.; Chang, H.-C.; Struve, W. S.; Atwell, G. J.; Denny, W. A. Excited-State Proton Transfers in 9-Aminoacridine Carboxamides. *J. Phys. Chem.* **1995**, *99*, 8927−8935.
(16) Demeunynck, M.; Charmantray, F.; Martelli, A. Interest of Acridine Derivatives in the Anticancer Chemotherapy. *Curr. Pharm. Des.* **2001**, *7*, 1703−1724.
(17) Brana, M. F.; Cacho, M.; Gradillas, A.; Pascual-Teresa, B.; Ramos, A. Intercalators as Anticancer Drugs. *Curr. Pharm. Des.* **2001**, *7*, 1745−1780.
(18) Kaur, J.; Singh, P. Acridine Derivatives: a Patent Review (2009−2010). *Expert Opin. Ther. Patents* **2011**, *21*, 437−454.
(19) Demeunynck, M. Antitumour Acridines. *Expert Opin. Ther. Patents* **2004**, *14*, 55−70.
(20) Denny, W. A. Chemotherapeutic Effects of Acridine Derivatives. *Med. Chem. Rev.* **2004**, *1*, 257−266.
(21) Belmont, P.; Bosson, J.; Godet, T.; Tiano, M. Acridine and acridone derivatives, anticancer properties and synthetic methods: Where are we now? *Anticancer Agents Med. Chem.* **2007**, *7*, 139−169.
(22) Langner, K. M.; Kedzierski, P.; Sokalski, W. A.; Leszczynski, J. Physical Nature of Ethidium and Proflavine Interactions with Nucleic Acid Bases in the Intercalation Plane. *J. Phys. Chem. B* **2006**, *110*, 9720−9727.
(23) Liu, C.; Jiang, Z.; Zhang, Y.; Wang, Z.; Zhang, X.; Feng, F.; Wang, S. Intercalation Interactions between dsDNA and Acridine Studied by Single Molecule Force Spectroscopy. *Langmuir* **2007**, *23*, 9140−9142.
(24) Hopcroft, N. H.; Brogden, A. L.; Searcey, M.; Cardin, C. M. X-Ray Crystallographic Study of DNA Duplex Cross-Linking: Simultaneous Binding to Two d(CGTACG)(2) Molecules by a Bis(9-aminoacridine-4-carboxamide) Derivative. *Nucleic Acids Res.* **2006**, *34*, 6663−6672.
(25) Brogden, A. L.; Hopcroft, N. H.; Searcey, M.; Cardin, C. J. Ligand Bridging of the DNA Holliday Junction: Molecular Recognition of a Stacked-X Four-Way Junction by a Small Molecule. *Angew. Chem., Int. Ed.* **2007**, *46*, 3850−3854.
(26) Finlay, G. J.; Atwell, G. J.; Baguley, B. C. Inhibition of the Action of the Topoisomerase II Poison Amsacrine by Simple Aniline Derivatives: Evidence for Drug-Protein Interactions. *Oncol. Res.* **1999**, *11*, 249−254.
(27) Nelson, E. M.; Tewey, K. M.; Liu, L. F. Mechanism of Antitumor Drug Action: Poisoning of Mammalian DNA Topoisomerase II on DNA by 4′-(9-acridinylamino)-methanesulfon-m-anisidide. *Proc. Natl. Acad. Sci. U.S.A.* **1984**, *81*, 1361−1365.
(28) Darzynkiewicz, Z.; Juan, G.; Srour, E. F. *Differential staining of DNA and RNA*; Robinson, J. P., Darzynkiewicz, Z., Dobrucki, J., Hyun, W. C., Nolan, J. P., Orfao, A., Rabinovitch, P. S., Eds.; *Current Protocols in Cytometry*; John Wiley & Sons: New York, 2004; Unit 7.3.
(29) Han, J.; Burgess, K. Fluorescent Indicators for Intracellular pH. *Chem. Rev.* **2010**, *110*, 2709−2728.
(30) Wang, Y.; Hu, X. Y.; Wang, L.; Shang, Z.-B.; Chao, J.-B.; Jin, W. A New Acridine Derivative as a Highly Selective 'Off-on' Fluorescence Chemosensor for Cd^{2+} in Aqueous Media. *Sens. Actuators B* **2011**, *156*, 126−131.
(31) Park, M. S.; Swamy, K. M. K.; Lee, Y. J.; Lee, H. N.; Jang, Y. J.; Moon, Y. H.; Yoon, J. A New Acridine Derivative as a Fluorescent Chemosensor for Zinc Ions in an 100% Aqueous Solution: a Comparison of Binding Property with Anthracene Derivative. *Tetrahedron Lett.* **2006**, *47*, 8129−8132.
(32) Bazzicalupi, C.; Bencini, A.; Matera, I.; Puccioni, S.; Valtancoli, B. Selective Binding and Fluorescence Sensing of Zn-II with Acridine-Based Macrocycles. *Inorg. Chim. Acta* **2012**, *381*, 162−169.
(33) Valeur, B. *Molecular Fluorescence*; Wiley-VCH, Weinheim, 2002.
(34) Balzani, V.; Bergamini, G.; Ceroni, P. From the Photochemistry of Coordination Compounds to Light-Powered Nanoscale Devices and Machines. *Coord. Chem. Rev.* **2008**, *252*, 2456−2469.
(35) Prodi, L.; Montalti, M.; Zaccheroni, N.; Dolci, L. S. *Topics in Fluorescence Spectroscopy*; Geddes, C. D., Lakowicz, J. R., Eds.; Springer: New York, 2005; Vol. 9, p 1.
(36) Fabbrizzi, L.; Licchelli, M.; Rabaioli, G.; Taglietti, A. The Design of Luminescent Sensors for Anions and Ionisable Analytes. *Coord. Chem. Rev.* **2000**, *205*, 85−108.
(37) Martinez-Mañez, R.; Sancenon, F. Fluorogenic and Chromogenic Chemosensors and Reagents for Anions. *Chem. Rev.* **2003**, *103*, 4419−4476.
(38) de Silva, A. P.; Gunaratne, H. Q. N.; Gunnlauson, T.; Huxley, A. J. M.; McCoy, C. P.; Rademacher, J. T.; Rice, T. E. Signaling Recognition Events with Fluorescent Sensors and Switches. *Chem. Rev.* **1997**, *97*, 1515−1566.
(39) Lodeiro, C.; Pina, F. Luminescent and Chromogenic Molecular Probes Based on Polyamines and Related Compounds. *Coord. Chem. Rev.* **2009**, *253*, 1353−1383.
(40) Lodeiro, C.; Capelo, J. L.; Mejuto, J. C.; Oliveira, E.; Santos, H. M.; Pedras, B.; Nuñez, C. Light and Colour as Analytical Detection Tools: A Journey into the Periodic Table Using Polyamines to Bio-

inspired Systems as Chemosensors. *Chem. Soc. Rev.* **2010**, *39*, 2948−2976.
(41) Bencini, A.; Lippolis, V. Probing Biologically and Environmentally Important Metal Ions with Fluorescent Chemosensors: Thermodynamic *Versus* Optical Response Selectivity in Some Study Cases. *Coord. Chem. Rev.* **2012**, *256*, 149−169.
(42) Formica, M.; Fusi, V.; Giorgi, L.; Micheloni, M. New Fluorescent Chemosensors for Metal Ions in Solution. *Coord. Chem. Rev.* **2012**, *256*, 170−192.
(43) Sessler, J. L.; Gale, P. A.; Cho, W. S. *Anion Receptor Chemistry*; Royal Society of Chemistry: Cambridge, 2006.
(44) *Supramolecular Chemistry of Anions*; Bowman-James, K., Bianchi, A., Garcia-España, E., Eds.; Wiley-VCH: New York, 2012. Gale, P.; Anslyn, E. V. Supramolecular Chemistry of Anionic species. *Chem. Soc. Rev.* **2010**, *39*, 3581.
(45) Fabbrizzi, L.; Licchelli, M.; Rabaioli, G.; Taglietti, A. The Design of Luminescent Sensors for Anions and Ionisable Analytes. *Coord. Chem. Rev.* **2000**, *205*, 85−108.
(46) Amendola, V.; Bonizzoni, M.; Esteban-Gomez, D.; Fabbrizzi, L.; Licchelli, M.; Sancenon, F.; Taglietti, A. Some Guidelines for the Design of Anion Receptors. *Coord. Chem. Rev.* **2006**, *250*, 1451−1470.
(47) Garcia-España, E.; Diaz, P.; Llinares, J. M.; Bianchi, A. Anion Coordination Chemistry in Aqueous Solution of Polyammonium Receptors. *Coord. Chem. Rev.* **2006**, *250*, 2952−2986.
(48) Mateus, P.; Bernier, N.; Delgado, R. Recognition of Anions by Polyammonium macrocyclic and Cryptand Receptors: Influence of the Dimensionality on the Binding Behavior. *Coord. Chem. Rev.* **2010**, *254*, 1726−1747.
(49) Katayev, E. A.; Ustynyuk, Y.; Sessler, J. L. Receptors for Tetrahedral Oxyanions. *Coord. Chem. Rev.* **2006**, *250*, 3004−3037.
(50) Kim, S. K.; Lee, D. H.; Hong, J.; Yoon, J. Chemosensors for Pyrophosphate. *Acc. Chem. Res.* **2009**, *42*, 23−31.
(51) Kang, S. O.; Hossain, M. A.; Bowman-James, K. Influence of Dimensionality and Charge on Anion Binding in Amide-Based Macrocyclic Receptors. *Coord. Chem. Rev.* **2006**, *250*, 3038−3052.
(52) Gunnlaugsson, T.; Glynn, M.; Tocci, G. M.; Kruger, P. E.; Pfeffer, F. M. Anion Recognition and Sensing in Organic and Aqueous Media Using Luminescent and Colorimetric Sensors. *Coord. Chem. Rev.* **2006**, *250*, 3094−3117.
(53) Lankshear, M. D.; Beer, P. D. Strategic Anion Templation. *Coord. Chem. Rev.* **2006**, *250*, 3142−3160.
(54) Gimeno, N.; Vilar, R. Anions as Templates in Coordination and Supramolecular Chemistry. *Coord. Chem. Rev.* **2006**, *250*, 3161−3189.
(55) Bazzicalupi, C.; Bencini, A.; Giorgi, C.; Valtancoli, B.; Lippolis, V.; Perra, A. Exploring the Binding Ability of Polyammonium Hosts for Anionic Substrates: Selective Size-Dependent Recognition of Different Phosphate Anions by Bis-macrocyclic Receptors. *Inorg. Chem.* **2011**, *50*, 7202−7216.
(56) Bazzicalupi, C.; Bencini, A.; Puccioni, S.; Valtancoli, B.; Gratteri, P.; Garau, A.; Lippolis, V. Selective Binding and Fluorescence Sensing of Diphosphate in H_2O via Zn^{2+}-Induced Allosteric Regulation of the Receptor Structure. *Chem. Commun.* **2012**, *48*, 139−141.
(57) Ambrosi, G.; Formica, M.; Fusi, V.; Giorgi, L.; Micheloni, M. Polynuclear Metal Complexes of Ligands Containing Phenolic Units. *Coord. Chem. Rev.* **2008**, *252*, 1121−1152.
(58) Di Giorgio, C.; De Meo, M.; Chiron, J.; Delmas, F.; Nikoyan, A.; Jean, S.; Dumenil, G.; Timon-David, P.; Galy, J.-P. Synthesis and Antileishmanial Activities of 4,5-di-Substituted Acridines as Compared to their 4-Mono-Substituted Homologues. *Bioorg. Med. Chem.* **2005**, *13*, 5560−5568.
(59) Bencini, A.; Burguete, M. I.; Garcia-España, E.; Luis, S. V.; Miravet, J. F.; Soriano, C. An Efficient Synthesis of Polyaza[n]-paracyclophanes. *J. Org. Chem.* **1993**, *58*, 4749−4753.
(60) Burla, M. C.; Caliandro, R.; Camalli, M.; Carrozzini, B.; Cascarano, G. L.; De Caro, L.; Giacovazzo, C.; Polidori, G.; Spagna, R. SIR2004: An Improved Tool for Crystal Structure Determination and Refinement. *J. Appl. Crystallogr.* **2005**, *38*, 381−388.
(61) Sheldrick, G. M. A Short History of SHELX. *Acta Crystallogr., Sect. A* **2008**, *64*, 112−122.
(62) Arca, M.; Bencini, A.; Berni, E.; Caltagirone, C.; Devillanova, F. A.; Isaia, F.; Garau, A.; Giorgi, C.; Lippolis, V.; Perra, A.; et al. Coordination Properties of New Bis(1,4,7-triazacyclononane) Ligands: A Highly Active Dizinc Complex in Phosphate Diester Hydrolysis. *Inorg. Chem.* **2003**, *42*, 6929−6939.
(63) Gran, G. Determination of the Equivalence Point in Potentiometric Titration, Part II. *Analyst* **1952**, *77*, 661−671.
(64) Gans, P.; Sabatini, A.; Vacca, V. Investigation of Equilibria in Solution. Determination of Equilibrium Constants with the HYPERQUAD Suite of Programs. *Talanta* **1996**, *43*, 1739−1753.
(65) Covington, A. K.; Paabo, M.; Robinson, R. A.; Bates, R. G. Use of the Glass Electrode in Deuterium Oxide and the Relation Between the Standardized pD (paD) Scale and the Operational pH in Heavy Water. *Anal. Chem.* **1968**, *40*, 700−706.
(66) Heyer, L. J.; Kruglyak, S.; Yooseph, S. Exploring Expression Data: Identification and Analysis of Coexpressed Genes. *Genome Res.* **1999**, *9*, 1106−1115.
(67) Chelli, R. Optimal Weights in Serial Generalized-Ensemble Simulations. *J. Chem. Theory Comput.* **2010**, *6*, 1935−1950.
(68) Chelli, R.; Signorini, G. F. Serial Generalized Ensemble Simulations of Biomolecules with Self-Consistent Determination of Weights. *J. Chem. Theory Comput.* **2012**, *8*, 830−842.
(69) Chelli, R.; Signorini, G. F. Erratum: Serial Generalized Ensemble Simulations of Biomolecules with Self-Consistent Determination of Weights. *J. Chem. Theory Comput.* **2012**, *8*, 2552−2552.
(70) Marsili, S.; Signorini, G. F.; Chelli, R.; Marchi, M.; Procacci, P. ORAC: A Molecular Dynamics Simulation Program to Explore Free Energy Surfaces in Biomolecular Systems at the Atomistic Level. *J. Comput. Chem.* **2010**, *31*, 1106−1116.
(71) Marcelli, A.; Foggi, P.; Moroni, L.; Gellini, C.; Salvi, P. R.; Jelovica Badovinac, I. Relaxation Properties of Porphyrin, Diprotonated Porphyrin, and Isoelectronic Tetraoxaporphyrin Dication in the S_2 State. *J. Phys. Chem. A* **2007**, *111*, 2276−2282.
(72) Moroni, L.; Gellini, C.; Salvi, P. R.; Marcelli, A.; Foggi, P. Excited States of Porphyrin Macrocycles. *J. Phys. Chem. A* **2007**, *112*, 11044−11051.
(73) Frisch, M. J.; Trucks, G. W.; Schlegel, H. B.; Scuseria, G. E.; Robb, M. A.; Cheeseman, J. R.; Scalmani, G.; Barone, V.; Mennucci, B.; Petersson, G. A., et al. *Gaussian 09, Revision A.1*; Gaussian, Inc.: Wallingford, CT, 2009.
(74) Tomasi, J.; Mennucci, B.; Cammi, R. Quantum Mechanical Continuum Solvation Models. *Chem. Rev.* **2005**, *105*, 2999−3094 and references therein.
(75) Richman, J. E.; Atkins, T. J. Nitrogen Analogs of Crown Ethers. *J. Am. Chem. Soc.* **1974**, *96*, 2268−2270.
(76) Smith, R. M.; Martell, A. E. *NIST Stability Constants Database*, version 4.0; National Institute of Standards and Technology: Washington, DC, 1997.
(77) Albert, A.; Goldacre, R. The Ionisation of Acridine Bases. *J. Chem. Soc.* **1946**, *68*, 706−713.
(78) Bencini, A.; Bianchi, A.; Garcia-España, E.; Micheloni, M.; Ramirez, J. A. Proton Coordination by Polyamine Compounds in Aqueous Solution. *Coord. Chem. Rev.* **1999**, *188*, 97−156.
(79) Bencini, A.; Bernardo, M. A.; Bianchi, A.; Fusi, V.; Giorgi, C.; Pina, F.; Valtancoli, B. Macrocyclic Polyamines Containing Phenanthroline Moieties - Fluorescent Chemosensors for H^+ and Zn^{2+} Ions. *Eur. J. Inorg. Chem.* **1999**, 1911−1918.
(80) Lodeiro, C.; Parola, J.; Pina, F.; Bazzicalupi, C.; Bencini, A.; Bianchi, A.; Giorgi, C.; Masotti, A.; Valtancoli, B. Protonation and Zn(II) Coordination by Dipyridine-Containing Macrocycles with Different Molecular Architecture. A Case of pH-Controlled Metal Jumping Outside−Inside the Macrocyclic Cavity. *Inorg. Chem.* **2001**, *40*, 2968−2975.
(81) Andres, A.; Bazzicalupi, C.; Bianchi, A.; Garcia-España, E.; Luis, S. V.; Miravet, J. F.; Rarnirez, J. A. Mono- and Bi-Nuclear Copper(II) Complexes of Azacyclophanes with a Single Aromatic Spacer. Crystal Structure of $[Cu_2L_2Cl_4]\cdot 5H_2O$ (L2 0 2,5,8,11-tetraaza[12]-paracyclophane). *J. Chem. Soc., Dalton Trans.* **1994**, 2995−3004.

(82) Andres, A.; Burguete, M. I.; Garcia-España, E.; Luis, S. V.; Miravet, J. F.; Soriano, C. Polyazacyclophanes - 2,6,9,13-Tetraaza[14]-paracyclophane as a Cationic and Anionic Receptor. *J. Chem. Soc., Perkin Trans.* **1993**, *2*, 749−755.
(83) Aguilar, J. A.; Díaz, P.; Doménech, A.; García-España, E.; Llinares, J. M.; Luis, S. V.; Ramírez, J. A.; Soriano, C. Synthesis, Protonation and Cu^{2+} Co-ordination Studies on a New Family of Thiophenophane Receptors. *J. Chem. Soc., Perkin Trans.* **1999**, *2*, 1159−1168.
(84) Kasama, K.; Kikuchi, K.; Yamamoto, S.; Ujl-le, K.; Nishida, Y.; Kokobun, H. Relaxation Mechanism of Excited Acridine in Non-reactive Solvents. *J. Phys. Chem.* **1981**, *85*, 1291−1296.
(85) Lindoy, L. F. *The Chemistry of Macrocyclic Ligand Complexes*; Cambridge University Press: Cambridge, UK, 1989.
(86) Bianchi, A.; Garcia-España, E. *Supramolecular Chemistry of Anions*; Bowman-James, K., Ed.; Wiley-VCH: New York, 2003.
(87) Studer, M.; Riesen, A.; Kaden, T. A. Metal-Complexes with Macrocyclic Ligands. 30. Synthesis and Structure of Halocuprates of Tetraprotonated 1,4,8,11-Tetraazacyclotetradecane and its Cu^{2+} Complex. *Helv. Chim. Acta* **1989**, *72*, 1253−1258.
(88) Micheloni, M.; Paoletti, P.; Vacca, A. Solution Chemistry of Macrocycles. Part 2. Enthalpic and Entropic Contributions to the Proton Basicity of Cyclic Tetra-amine Ligands: 1,4,8,11-Tetra-azacyclotetradecane, 1,4,8,12-Tetra-azacyclopentadecane, and 1,4,8,11-Tetramethyl-1,4,8,11-tetra-azacyclotetradecane. *J. Chem. Soc., Perkin Trans. II* **1978**, 945−947.